Science of the Total Environment 924 (2024) 171489

Contents lists available at ScienceDirect

Science of the Total Environment

journal homepage: www.elsevier.com/locate/scitotenv

Prolonged drought periods over the last four decades increase flood intensity in southern Africa

Fulvio Franchi [a,b,c,*], Syed Mustafa [d], Daniel Ariztegui [e], Farisse J. Chirindja [f], Andrea Di Capua [g,h], Stephen Hussey [i], Jean-Luc Loizeau [e], Vittorio Maselli [j], Alessia Matanó [k], Oluwaseun Olabode [l], Florian Pasqualotto [h], Whatmore Sengwei [m], Sithabile Tirivarombo [b], Anne F. Van Loon [k], Jean-Christophe Comte [l,**]

[a] Earth and Environmental Science Department, Botswana International University of Science and Technology, Private Bag 16, Palapye, Botswana
[b] Dipartimento di scienze della Terra e Geoambientali, Università degli studi di Bari - Aldo Moro, Bari, Italy
[c] School of Geosciences, University of the Witwatersrand, Braamfontein, 2001 Johannesburg, South Africa
[d] Hydrology and Quantitative Water Management Group, Wageningen University & Research, the Netherlands
[e] Department of Earth Sciences, University of Geneva, Rue des Maraichers 13, 1205 Geneva, Switzerland
[f] Geology Department, Eduardo Mondlane University, Av. Mozambique km 1.5, P.O. Box 273, Maputo, Mozambique
[g] CNR IGAG – Institute of Environmental Geology and Geoengineering, Via M. Bianco 9, 20131 Milan, Italy
[h] University of Insubria, Department of Science and High Technology, Via Valleggio 11, Como, Italy
[i] Dabane Trust, 13 Cathkin Ln, Bulawayo, Zimbabwe
[j] Dipartimento di Scienze Chimiche e Geologiche, Università degli Studi di Modena e Reggio Emilia, Modena, Italy
[k] Vrije Universiteit, Institute for Environmental Studies, De Boelelaan 1111, 1081 HV Amsterdam, the Netherlands
[l] School of Geosciences, University of Aberdeen, King's College, AB24 3FX Aberdeen, UK
[m] Mathematic and Statistics Department, Botswana International University of Science and Technology, Private Bag 16, Palapye, Botswana

HIGHLIGHTS

- Sedimentary and hydrological data were coupled to study floods/droughts in the LRB.
- Land use changes impacted river flow modifying the natural interannual oscillation.
- Severity and frequency of floods correlate with increasing severity of droughts.
- Increasing severity of flood correlates with long-term decline in groundwater.
- Intense floods correlate with wetter-than-normal periods following prolonged droughts.

GRAPHICAL ABSTRACT

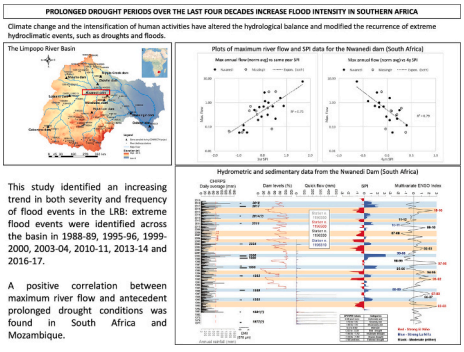

ARTICLE INFO

Editor: Ouyang Wei

ABSTRACT

In semi-arid sub-Saharan Africa, climate change and the intensification of human activities have altered the hydrological balance and modified the recurrence of extreme hydroclimatic events, such as droughts and floods.

* Corresponding author at: Dipartimento di scienze della Terra e Geoambientali, Università degli studi di Bari - Aldo Moro, Bari, Italy.
** Corresponding author.
E-mail addresses: fulvio.franchi@uniba.it, franchif@biust.ac.bw (F. Franchi), jc.comte@abdn.ac.uk (J.-C. Comte).

https://doi.org/10.1016/j.scitotenv.2024.171489
Received 20 September 2023; Received in revised form 3 March 2024; Accepted 3 March 2024
Available online 5 March 2024

Keywords:
Limpopo River
Transboundary basins
Floods
Droughts
Dam sediments

The geomorphological heterogeneity of river catchments across the region, the variable human pressure, and the lack of continuous hydroclimatic data preclude the definition of proper mitigation strategies, with a direct effect on the sustainability of rural communities.

Here, for the first time in Africa, we characterize hydrological extreme events using a multidisciplinary approach that includes sedimentary data from dams. We focus on the Limpopo River basin to evaluate which factors control flood magnitude since the 1970. Extreme flood events were identified across the basin in 1988–89, 1995–96, 1999–2000, 2003–04, 2010–11, 2013–14 and 2016–17. The statistical analysis of sedimentary flood records revealed a dramatic increase in their magnitude over the studied period. A positive correlation between maximum river flow and antecedent prolonged drought conditions was found in South Africa and Mozambique. Most importantly, since 1980, we observed the likely decoupling of extreme floods from the magnitude of La Niña events, suggesting that the natural interannual variability driven by El Niño-Southern Oscillation (ENSO) has been disrupted by climate changes and human activities.

1. Introduction

Extreme hydrological events, such as floods and droughts, can negatively affect the development of societies and their economies, and result in significant loss of life and livelihoods (Carleton and Hsiang, 2016). This is particularly true in developing countries, which are less prepared and resilient to such natural disasters. In the last few decades, the frequency and intensity of hydrological extreme events drifted away from the natural interannual variability modes, such as El Niño climate oscillation, due to increasing global temperatures (e.g., Trambauer et al., 2015; Maposa et al., 2016). An increasing number of studies have concluded that climate change will lead to an increase in the magnitude and frequency of extreme events (Easterling et al., 2000; Hamlet and Lettenmaier, 2007; Vanniere et al., 2013).

In African semi-arid basins, the effects of extreme hydrological events on infrastructure and livelihoods have been exacerbated by increasing human activities that have led to significant alternation of the natural environment (e.g., Stott, 2016; Sorensen et al., 2021). In southern Africa, where people rely primarily on rain-fed agriculture, natural climatic variability has a profound effect on food availability. This is further compounded by the effects of climate warming which predicted to increase the frequency of flood and drought events (Talafre and Knabe, 2009). In Southern African, problematically, the accuracy of studies of hydrological extremes is often poor due to the lack of continuous hydro-meteorological time series data (Spaliviero et al., 2014; Sorensen et al., 2021). Moreover, the physical connectivity of such large transboundary basins is seldom considered (Spaliviero et al., 2014), i.e. surface water and groundwater are often studied as separate entities, even when the interaction between the two has been clearly recognised (Partington et al., 2017; Geris et al., 2022).

Hydrological extreme events (hazards) are usually identified using pre-set exceedance thresholds of hydrometric parameters. Floods magnitude, in particular, is often calculated using models based on river discharge time series (Trigg et al., 2016; Devitt et al., 2021). Recent advances in sedimentology offer a new approach based on sedimentary archives to develop continuous, quantitative, and event-scaled records of past flood frequency and magnitude, thus allowing a comparison with hydrometric data and climate models (Toonen et al., 2015; Munoz et al., 2018). Although, the sediments balance approach has proven to be crucial for detecting flood events and studying their impact on soil erosion and ecosystems, this method is often neglected in African rivers monitoring systems.

Our knowledge about spatial distribution, forcing factors and severity of extreme hydrological events (droughts and floods) in the LRB and their potential impacts comes from studies made a posteriori, when it is too late for mitigation measures (e.g., Spaliviero et al., 2014). All existing information on the impacts of extreme hydrological events comes from available hydrometric data collected over the past 40–50 years (Alemaw et al., 2013; Trambauer et al., 2015; Maposa et al., 2016). No attempt to use geological proxies to extend the time series backward in time has been done yet and few climate projections have been attempted (Botai et al., 2020).

This study aims to reconstruct the spatial and temporal variability and severity of hydrological extreme events across the Limpopo River Basin (LRB), as an analogues for other semi-arid sub-Saharan river basins. To reach this goal, we introduced a novel approach that combines sedimentary records from artificial reservoirs within the LRB with available hydroclimatic data, including in-situ river discharge and satellite rainfall data, along with reports on extreme events (Spaliviero et al., 2014; Trambauer et al., 2015; Lindevall, 2017; Botai et al., 2020). By quantifying the timing and magnitude of floods and droughts that have occurred since the 1970s, this study will provide insights into the climate mechanisms governing these extreme atmospheric events. The knowledge gained has the potential to enhance future forecasting capabilities, ultimately increasing the resilience of developing countries to climate extremes.

2. Materials and methods

2.1. Study area

The LRB stretches for 415,00 km^2 across Botswana, South Africa, Zimbabwe and Mozambique (Fig. 1) and is characterized mainly by arid to semi-arid climate with overall aridity decreasing downstream (Spaliviero et al., 2014; Trambauer et al., 2015). The Limpopo River sustains the livelihood of about 14 million people across the four riparian countries and it is considered to be under constant water stress (Trambauer et al., 2015; Botai et al., 2020). In the LRB the dominant land cover classes are savannah-grass and shrublands (Kim et al., 2023).

The population is unevenly distributed with sparsely populated areas and large capital cities (e.g. Gaborone and Pretoria in Botswana and South Africa, respectively). Increasing urbanization and development in the basin led to a rapid increase of human activities with consequent increase of vulnerability in the flooding areas (Spaliviero et al., 2014). The mean annual rainfall in the basin ranges between 200 and 1200 mm/yr with an average across the basin of 530 mm/yr (Alemaw et al., 2013; Trambauer et al., 2015; Mosase and Ahiablame, 2018). The LRB is characterized by high geological heterogeneity (Fig. 1B); a detailed geodynamic, structural and morphological review of the basin in provided in Spaliviero et al. (2014).

The upper reach of the Limpopo River flows across the highlands of south-eastern Botswana, where the volcano-sedimentary units of the Transvaal Supergroup and the Gaborone Granite are exposed (Franchi and Mapeo, 2019) (Fig. 1B). For most of its upper course between eastern Botswana, South Africa and Zimbabwe, the Limpopo River drains crystalline rocks of the Kaapvaal Craton, Bushveld Igneous Complex, Limpopo mobile belt and Zimbabwe Craton (e.g., Rollinson and Blenkinsop, 1995; Barton et al., 2006) (Fig. 1B). The right bank tributaries of the Limpopo River flow through the sedimentary units of the Upper Karoo Supergroup (e.g., Catuneanu et al., 2005) and Transvaal Supergroup (Bumby et al., 2012). The left bank tributaries of the Limpopo River flow through the unconsolidated sediments of the Kalahari Group overlying the volcano sedimentary units of the Karoo Supergroup and the sedimentary units of the Palapye Group and Waterberg

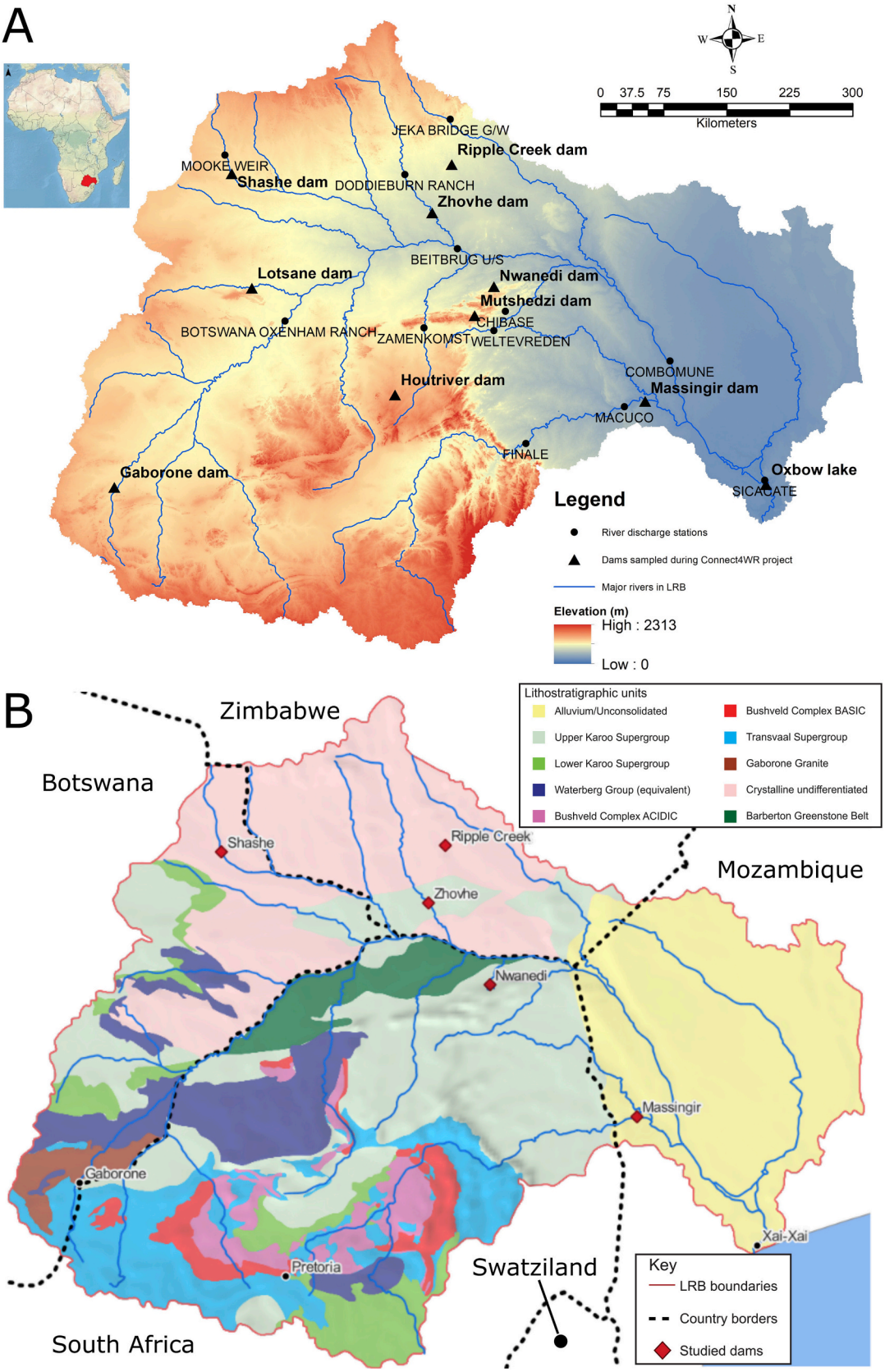

Fig. 1. A) Digital Elevation model of the Limpopo River Basin in Southern Africa (red in the inset) showing the main Limpopo River tributaries and the dams sampled during CONNECT4 Water Resilience project. The River discharge stations are indicated by the 7 digits numbers. B) Simplified geological map of the Limpopo River Basin. Geology of Botswana modified from the 1998 digital edition of the Geological map of Botswana (Key and Ayers, 2000). Geology of Mozambique modified from Ruotoistenmäki (2008). Geology of South Africa modified from Vorster (2005). Geology of Zimbabwe modified from Stagman (1984).

Group-equivalent (Mapeo et al., 2004) in Botswana (Fig. 1B). The lower reach of the river, in Mozambique, flows through mostly unconsolidated alluvium until it reaches the Indian Ocean near Xai-Xai in Mozambique (Fig. 1B).

The focus of this work is on 4 sub-catchments representative of different geological, hydrological and climatic conditions across the LRB: Shashe (Botswana), Nwanedi (South Africa), Ripple Creek (Zimbabwe) and Massingir (Mozambique). The Shashe Dam is an embankment dam along the Shashe river with a total capacity of 8.5×10^7 m^3. The Nwanedi Dam is an arch type dam along the Nwanedi river with a total capacity of 5.3×10^6 m^3 (Lombaard et al., 2015). The Ripple Creek Dam is an embankment dam on the Bubiana river, though very little information is available for this reservoir that is found within a private game reserve. The Massingir Dam is an embankment dam along the Olifants river with a total capacity of 2.88 km^3 (Limpopo Basin Permanent Technical Committee, 2010).

2.2. Samples collection and analyses

Sediment cores were collected from a raft (a floating platform propelled by oars) using a gravity corer with percussion hammer and polycarbonate core barrels of 68 mm in diameter and 1.5 m in length. Most of the cores have a total recovery <20 cm, and here we are presenting only the results from the most representative (i.e. longer and complete) cores. When possible, cores were x-ray scanned before splitting, with average working conditions: ca. 70 mV and 6.30 mAs. Cores were further described and sampled every 1 cm; at least one core for each reservoir was analysed for grain size and organic matter distribution (Franchi et al., 2023). Sample intervals were adjusted to correspond with visual and x-ray flood couplets. Where flood layers were thinner than 1 cm, they were not sampled individually, due to the minimum required sample volume for grain size, organic matter and dating analysis. Grain size analysis was carried on wet samples dispersed in water and analysed with a Malvern Mastersizer 3000 laser diffraction particle size analyser at Botswana International University of Science and Technology (BIUST), Palapye (Botswana). Few grams of the samples were dispersed into a glass container with half a spoon of sodium hexametaphosphate to prevent clays from flocculation. The organic matter content was determined using Loss on Ignition (LOI) method whereby the wet samples from the cores were dried at 60 °C for 24 h and weighed. The dried samples were placed in the funnel furnace at 550 °C for 2 h and then weighed again to determine LOI.

2.3. Sediments as proxy for the study of hydrological events

Sediments are an important component of the natural environment and play a major role in and around aquatic systems. To sustainably maintain the integrity of an ecosystem there must be a state of dynamic equilibrium between sediment aggradation and degradation in a catchment. However, human interferences tend to upset the balance resulting in impaired ecosystems and consequently increasing the vulnerability of riparian communities (e.g., Booth and Henshaw, 2001). Activities such as sand river mining, hydropower generation projects, inappropriate agricultural management can alter the sediment load in a catchment, thus impacting sediment and hydrological balances.

Although it has proven to be a crucial aspect for the study of the impact of extreme events on soil erosion and ecosystems, the sediment balance is often neglected in monitoring systems on African rivers (Coppus and Imeson, 2002; see Owens, 2020 for a review). The extreme (or severe) events can in fact enhance debris-flow occurrence and lead to pulses of sediment into the rivers and, eventually, alter the hydrodynamics and physiography of the river and of the natural and artificial lakes and reservoirs within the basin (e.g., Goode et al., 2012; Franchi et al., 2020) affecting human activities. Therefore, an improved understanding of the temporal and spatial variations of sediments delivered into a catchment and the problems associated with sediment transport is required for the sustainable management of catchment resources. This can be done through a monitoring programme that establishes the long-term variability in sediment budgets across sections of the catchment after which the trends can be assessed in relation to activities within the catchment (Haimann et al., 2014; Walling and Fang, 2003).

The sediments within the LRB reservoirs are archives of local hydrological and weather events providing insights into the different sub-catchments across the LRB. These sediments offer: i) an overview across the basin of the major flood events and their magnitude; ii) their recurrence and predictability, i.e. how much rain can cause a flood in the LRB; iii) the effects of El Niño-Southern Oscillation (ENSO) on the severity of floods.

2.4. CHIRPS and peak over threshold (POT)

Climate Hazards Group InfraRed Precipitation with Station (CHIRPS) (Funk et al., 2015) datasets are used to analyse rainfall based extreme weather events. CHIRPS is a multi-satellite precipitation product with a high spatial resolution (0.05°) that uses in-situ station data for bias adjustment and creates a gridded rainfall time series. The CHIRPS Precipitation is widely used for long-term precipitation and hydrological extreme analyses. Recent studies from different part of the world shows that CHIRPS data can be used with higher confidence in hydrological extreme analyses (Nkunzimana et al., 2019; Wu et al., 2019). In this study, the daily CHIRPS precipitation data from 1981 to 2020 were collected from https://data.chc.ucsb.edu/products/CHIRPS-2.0/ (last accessed on 10 December 2021). The maximum daily rainfall and the total annual rainfall were calculated by averaging the CHIRPS rainfall data on the nodes falling within the dams' upstream sub-catchments (Figs. 3–6).

Daily in-situ river discharge data at 77 stations within the LRB (Fig. 1A) were collected from the Global Runoff Data Centre (GRDC). The time series length was different for each station based on data availability. The GRDC is an international data centre in Germany operating under the support of the World Meteorological Organization (WMO).

River discharge based extreme flow (floods) analysis was carried out using the Peaks Over Threshold (POT) method as it allows for a more rationalized selection of floods (Lang et al., 1999). The POT values were defined as peak flows (discharges) greater than a selected threshold. In this study, we select the threshold based on physical identification of the river levels leading to flood inundation whereby the river overflows in its adjacent floodplain. The rationale for this approach is (1) floods leading to floodplain inundation are those that cause most damages, and (2) these floods are associated to more extensive and unambiguous sediment records. The overflow level for a specific river was directly identified based on the historical flood record (Lindevall, 2017), i.e. if there was an historical flood recorder the threshold for flooding was taken at that specific time and place. In this way the selected threshold flood level effectively captures all historical flood events. In order to provide independent events, hydrographs series were processed using WETSPRO (Willems, 2009), where the independent events were selected after the separation of slow and quick flow. Measurements of river discharge were considered as leading to floods when exceeding the POT, heavy floods when exceeding twice the POT value, and severe floods when exceeding three times the POT value.

2.5. Drought events detection

A variable threshold analysis was carried out to detect drought events that are hereby defined as low flow periods (Table 1 and Supplementary Online Material 1). Different variable thresholds related to the 80th, 90th, 95th and 99th percentile were identified. The resulting low flow events were compared with recorded drought events from literature (Table 1 and S.O.M. 1). The largest positive correlation with recorded drought events was for analysis run using a threshold of 0.8

(80th percentile). The 80th percentile was therefore used as thresholds for the final analysis to focus on extreme low events.

The annual Standardized Precipitation Index (SPI; McKee et al., 1993) and Standardized Precipitation Evapotranspiration Index (SPEI; Vicente-Serrano et al., 2010) were used to identify meteorological droughts. The daily Climate Hazards Group InfraRed Precipitation with Station (CHIRPS; Funk et al., 2015) data from 1981 to 2020 have been used to calculate SPI. Precipitation data were coupled with evapotranspiration data to calculate SPEI. The actual evapotranspiration and interception (ETIa-WPR) data from 2009 to 2020 were collected from the FAO Water Productivity Open-access portal (WaPOR; FAO, 2020). While the CHIRPS data used for SPI calculation are available from the 80s, the evapotranspiration data for SPEI calculation in the region are available only from 2009.

2.6. Radiometric dating and age model

Ten freeze-dried sediment samples from core N5 and six samples from core B1 were measured for ^{137}Cs activity at 661 keV using an Ortec-EGG (Oak Ridge TN) High-Purity, Germanium Crystal Well, Photon Detector (Well Detector) coupled to a Digital Gamma-Ray Spectrometer (Dspec) at the Science Museum of Minnesota, USA (S.O.M. 2). The activity of ^{137}Cs in core M10 was obtained using a HPGe well gamma spectrometer (Ortec EG&G) measuring gamma emissions at 46.5 keV and 662 keV respectively, at the Department F.-A. Forel of the University of Geneva, Switzerland (S.O.M. 2).

Approximately 4.7 cm^3 of sediment were packed into a 1 cm × 10 cm polycarbonate tube and sealed with a plastic cap. Cesium-137 detection methods are based on (Ritchie and McHenry, 1973). Cesium-137 activity is quantified using *GammaVision* software, which incorporates user defined energy and efficiency standard calibrations.

The ^{137}Cs isotope is used as a stratigraphic marker of peak atmospheric nuclear weapons testing before the Nuclear Weapons Treaty which banned these tests. Additionally, ^{137}Cs was released into the atmosphere during the 1986 Chernobyl nuclear disaster and provides a secondary marker in areas of the globe where detectable fall-out occurred.

The rise in ^{137}Cs activity in the Southern Hemisphere has been dated as starting around 1958 (Longmore, 1982; Foster et al., 2005). Subsequently, the fallout related to the atmospheric thermonuclear bomb testing in this hemisphere reached a peak in 1965, whereas the Chernobyl peak at 1986 has never been unambiguously reported from this part of the world (Evrard et al., 2020). In the sediments from Nwanedi Dam, the only site for which there is a complete ^{137}Cs record, radiocaesium shows a strong positive peak near the floor of the dam, at depth of ca. 50 to 45 cm (Fig. 2). Considering that the dam was opened in 1966, this peak is interpreted as the thermonuclear bomb testing fallout of the mid 60s as accumulated in the top soils (Fig. 2). The peak at around 45 cm depth is characterized by a drop in ^{137}Cs activity due to an increase in grain size as radio cesium is preferentially bound to the fine fraction (He and Walling, 1996). The initial years after the dam construction were probably characterized by a very low depositional rate due to partial filling of the dam (and consequent sediment erosion). The low water levels in the early years of the Nwanedi Dam could be explained by the prolonged dry spell that occurred at the beginning of the dam operation (1967–1973; Fig. 2 and Table 1). The top 50–45 cm of sediments preserved in the core represent, therefore, ca. 60 years of deposition. The gradual decrease of ^{137}Cs toward the top demonstrate an increase in soil erosion culminated in the last decade (Evrard et al., 2020).

The ^{137}Cs from the Ripple Creek Dam sediments showed values below the detection limit (S.O.M. 2). Two ^{137}Cs values, at 5 and 13 cm depth (S.O.M. 2), fall within the activity concentrations of 4 mBq g^{-1} reported in one of few studies conducted in the region by Owens and Walling (Owens and Walling, 1996). These values are comparable with the superficial sediments found in Nwanedi Dam (Fig. 2).

Activities of ^{210}Pb in core M10 were determined on 23 samples using a HPGe well gamma spectrometer (Ortec EG&G), measuring gamma emissions at 46.5 keV (^{210}Pb), 295.2 and 351.9 keV (^{214}Pb). Prior to the ^{210}Pb analysis, samples were prepared as described in Appleby (2001). The detection efficiency was adjusted for geometry, density and chemical composition using Monte Carlo simulation software (Gespecor 4.1, Sima et al., 2001). The age model was based on the constant initial concentration dating model (Appleby, 2001). As the sediment sequence at the top of the core was lost during the coring operation, the initial $^{210}Pb_{xs}$ activity was estimated by extrapolation toward the core top using the $^{210}Pb_{xs}$ decay rate between 28 and 41 cm, assuming that 10 cm of sediment was lost, and that the sediment layer between 10 and 28 cm was deposited in a single event. Massingir Dam was opened in 1975 but never completed until work restarted in 1994 and completed in 2007. This same year the entire western part of the dam was dry.

The dams in Botswana have been constructed after the 1960s, thus the stratigraphic record present within the reservoirs is too recent to successfully apply ^{137}Cs and ^{210}Pb techniques. Consequently, the age model of the basin is obtained using the time series of sedimentary floods, as outlined in Fig. 6.

Considering the limitations of using short-lived isotopes such as ^{210}Pb and for ^{137}Cs for dating the sediments accumulating within the reservoirs, the age-depth model for each dam was done iteratively (Toonen et al., 2015) integrating the available radiometric dating results with: i) date of collection of the core and date of construction of the dams; ii) age assigned to largest flood events; and iii) other flood events assigned to minor sedimentological flood records as outlined in Figs. 2–6. This model starts from the assumption that the larger floods will correspond with the coarsest beds in the cores (cf. Toonen et al., 2015). Peak in the grain size profile were correlated with confirmed historical events starting from the most recent and repeated until all major floods for the past 40–50 years were assigned to a flood layer.

Two events were identified as marker events in each core, i.e. the floods of 2000 and the floods linked with Cyclone Dineo in 2017, as there are both hydrometric data and sedimentological flood indicators in each one of the sub-basin considered in this study (Table 1 and S.O.M. 1). Bearing in mind that all the samples were collected during 2018 dry season, the 2017 event was assigned to the topmost flood couplet in each core (Figs. 2–6). The 2000 event was assigned to the peak with higher coarse-EM scores in the record as this was the period with higher precipitation and POT across the region (Figs. 2–6).

2.7. End Member Modelling and Flood magnitude

The individual flood events preserved in the sediment cores were identified by using grain-size analysis and x-ray imaging of the cores (where available) and organic matter contents (Figs. 2, 4–6). The grain size distribution of the sediments was analysed using the End Members Modelling Analysis (EMMA) algorithm and the method presented in Weltje and Prins (2007) and applied to the estimation of flood magnitudes as in Toonen et al. (2015) and Munoz et al. (2018). The original EMMA algorithm for grain-size distribution was published by Dietze et al. (2012) and it was based on principal component analysis (PCA), factor rotation, variable data scaling and non-negative least-square estimation (Hartmann et al., 2023). Only the longest and best-preserved cores were selected for EMMA analysis. The limited number of grain size measurements from shorter cores might have flawed the model as the greater is the sample size the lower is the effect of outliers and more robust are the End Members (Hartmann pers. Comm., 2021).

The EMMAgeo package was available at www.geo.fu-berlin.de (Hartmann et al., 2023). This algorithm provides a set of functions for EM modelling analysis of grain-size data to calculate discrete and robust end members. The technique classifies grain size datasets into a series of distinct grain size populations from which a physical meaning can be assigned on sedimentological and hydrological grounds (Toonen et al., 2015). EMMAgeo algorithm provides an optimum number of EM which can best explain the variability in the dataset as such, any addition of EM

Table 1
Summary of the floods and drought events reported in literature for the LRB. CHIRPS data showing the daily average and the annual mean over the selected dam sub-basins in the four riparian countries. CHIRPS values in bold are exceeding the thresholds of the 99th percentile on the average daily rainfall: Nwanedi Dam 99th percentile on the average daily rainfall = 73 mm/day; average annual rainfall = 683 mm/yr. Ripple Creek Dam 99th percentile on the average daily rainfall = 37 mm/day; average annual rainfall = 445 mm/yr. Massingir Dam 99th percentile on the average daily rainfall = 36 mm/day; average annual rainfall = 494 mm/yr. Shashe Dam 99th percentile on the average daily rainfall = 25 mm/day; average annual rainfall = 437 mm/yr.
ENSO data from Baddoo et al. (2015) and from origin.cpc.ncep.noaa.gov. Reported effects of the extreme events from Trambauer et al. (2015), Spaliviero et al. (2014), Wessels et al. (2004), Fitchett and Grab (2014), Rapolaki and Reason (2018) and Reason (2007), and from Lindevall (2017) if not otherwise stated. Drought condition were reported when the average monthly discharge value from at least two stations was equal to or below the threshold and this condition was protracted for at least 2 consecutive months.

Year	ENSO	BW	MOZ	SA	ZIM	Region	Reported flood/drought effects
Flood	La Niña	CHIRPS (max daily average/annual total average) [mm]					
		26/ 437	36/ 494	73/683	37/ 445		
1977		N/A	N/A	N/A	N/A	Mozambique	300 deaths - ca. 400,000 people affected
1981		***46***/ 363	*37*/ 494	***108***/ ***827***	***54***/ ***492***	Basin	>500,000 people affected
1985		24/ 363	***57***/ ***597***	55/ ***855***	26/ ***498***		
1988–89	Strong	***29***/ ***482***	***37***/ 410	***77***/631	***39***/ ***455***		
1993–94		18/ 333	***38***/ ***502***	65/ ***742***	*37*/ **537**		Cyclone Nadia in Mozambique - 204 dead, 1.5 million homeless, $240 million damage (Fitchett and Grab, 2014; Rapolaki and Reason, 2018)
1995–96	Moderate	***67***/ ***578***	***55***/ ***731***	***77***/ ***1074***	***48***/ ***612***	Basin	Cyclone Bonite - ca. 200,000 people affected (Trambauer et al., 2015; Wessels et al., 2004)
1998–99	Moderate	25/ 357	***45***/ ***595***	44/ ***686***	***43***/ ***469***	Basin	
1999–00	Strong	***55***/ ***767***	***68***/ ***940***	***117***/ ***1439***	***56***/ ***719***	Basin	Cyclone Eline - 150 dead from storm, total 1000 casualties from flooding, 300,000 displaced, 4 ships sunk in Mozambique (Fitchett and Grab, 2014; Rapolaki and Reason, 2018; Trambauer et al., 2015; Wessels et al., 2004)
2000–01		***27***/ 434	***47***/ ***625***	68/636	***42***/ ***489***	Mozambique	Cyclone Dera - 100 deaths, 250,000 displaced, severe flooding (Fitchett and Grab, 2014; Reason, 2007).
2002–03		25/ 320	21/ 362	49/565	***82***/ ***449***	Mozambique	Cyclone Delfina (February) - 76 deaths, 22,000 displaced, several days power outage, $3.5 million in damage Cyclone Japhet (March)- 17 dead, 23,000 homeless, 237,000 ha cropland destroyed, livestock losses (Fitchett and Grab, 2014; Rapolaki and Reason, 2018)
2003–04		23/ 419	*36*/ ***574***	71/ ***790***	***57***/ ***536***	Mozambique + Zimbabwe	
2006–07		***25***/ ***678***	***51***/ ***574***	49/ ***721***	33/ ***515***	Mozambique	Cyclone Favio - 10 dead, 100 injured, 33,000 homeless, $71 million in damage (Fitchett and Grab, 2014; Rapolaki and Reason, 2018)
2007–08	Strong	***26***/ 384	24/ 400	67/543	28/ 297	Mozambique	Cyclone Jokwe - 16 dead, 55,000 homeless, 75 % of power lines in Nampula destroyed (Fitchett and Grab, 2014; Rapolaki and Reason, 2018)
2010–11	Strong	**28**/ **470**	**48**/ 490	62/***759***	35/ **511**		
2011–12	Moderate	24/ 292	***46***/ 475	54/451	25/ 242	Mozambique	Cyclone Funso - 15 dead from ship sinking, 56,000 homeless, 70,000 with no access to clean drinking water (Fitchett and Grab, 2014; Rapolaki and Reason, 2018)
2012–13		24/ 350	***57***/ ***638***	***96***/ ***848***	***57***/ ***529***	Mozambique + Botswana	150,000 people displaced - 100 casualties in Mozambique; 842 families affected; 400 people displaced; heavy damages to infrastructures and livestock in Botswana.
2013–14		***29***/ ***598***	***37***/ ***567***	***87***/ ***771***	***61***/ ***626***	South Africa	7000 people affected; 32 deaths; 3525 were displace; heavy damages to infrastructures in South Africa. people were displaced in Mozambique (Spaliviero et al., 2014).
2014–15		23/ 281	22/ 334	30/403	***58***/ 268	Mozambique + Zimbabwe	Tropical storm Chedza (Rapolaki and Reason, 2018). 408,711 people affected in Mozambique and 6000 in Zimbabwe; 68,000 people displaced in Mozambique.
2017		***30***/ ***740***	***57***/ ***572***	***98***/ ***967***	***63***/ ***739***	Basin	Cyclone Dyneo caused 246 deaths and damages to infrastructures in excess of $100 million.

Year	ENSO	Botswana	Mozambique	South Africa	Zimbabwe	Region	Reported flood/drought effects
Drought	El Niño	CHIRP (annual total averaged) [mm]					
		437	500	683	445		
1978		N/A	N/A	N/A	N/A		
1979		N/A	N/A	N/A	N/A		Prolonged drought reported by Schulze (1984).
1980		N/A	N/A	N/A	N/A		
1982–83	Strong	321	409	516	353	Botswana, Mozambique	ca. 2.46 million people under food insecurity threshold (Schulze, 1984).
1985		363	***597***	***855***	***497***	Botswana and South Africa	Below average rainfalls reported by Wessels et al. (2004).
1986–87	Moderate	419	440	656	402	Botswana, South Africa, Zimbabwe	Drought reported by Schulze (1984); below average rainfalls reported by Wessels et al. (2004).
1987–88	Strong	***438***	444	648	394	Botswana and South Africa	Below average rainfalls reported by Wessels et al. (2004).

(*continued on next page*)

Table 1 (*continued*)

Year	ENSO	Botswana	Mozambique	South Africa	Zimbabwe	Region	Reported flood/drought effects
Drought	El Niño	CHIRP (annual total averaged) [mm]					
		437	500	683	445		
1990		338	***531***	588	***458***	Botswana and South Africa	Drought reported by Schulze (1984).
1991–92	Strong	352	404	654	379	Basin	ca. 1.5 million people affected in Mozambique; violent epidemic of cholera. Drought reported by Schulze (1984); below average rainfalls reported by Wessels et al. (2004).
1994–95	Moderate	360	401	*530*	395		Drought reported by Schulze (1984); below average rainfalls reported by Wessels et al. (2004).
1997–98	Strong	423	**609**	*673*	**505**		Drought reported by Wessels et al. (2004).
2002–03	Moderate	261	323	462	329	Mozambique	520,000 people facing food insecurity. Drought reported by Schulze (1984); below average rainfalls reported by Wessels et al. (2004).
2005–06		***548***	436	565	404		Drought reported by Schulze (1984).
2009–10	Moderate	***486***	***525***	***762***	***456***		
2015–16	Strong	***479***	457	557	406	Basin	Ca.22 million people under food insecurity; release of water from Massingir Dam.

beyond the optimum number did not lead to a significant improvement in the total amount of variability explained by the mixing model. This implies that addition of EM would not have any geological interpretations (Prins et al., 2000).

Due to the differences in the location of the sites where the data has been collected, different optimum numbers of EM were obtained for each site (S.O.M. 3). For characterizing flood magnitudes, we considered only the two coarsest end members for each dataset (Figs. 2, 4–6). The algorithm accounts for the distinct phasing in the accumulation of sediments fills by normalizing the dataset to allow for a uniform treatment of samples coming from different phases of sedimentation. Toonen et al. (2015) argued that without this normalization, a phase with a relatively-nearby position of the active river would be mistaken for a period with large floods. Grain size was normalized into z-scores (score columns in Figs. 2, 4–6) per end member and this allows for the unification of data across different end members.

3. Results

3.1. Extreme flood events in the LRB

The LRB experienced a series of devastating hydrological extreme events throughout the study period. The observations for the 40 years between 1977 and 2017, summarized in Table 1, show the occurrence and impact of hydrological floods and droughts from literature (Spaliviero et al., 2014; Trambauer et al., 2015; Lindevall, 2017; Botai et al., 2020) coupled with the evidences from the available hydroclimatic data and POT values (see also S.O.M. 1).

The most complete data set of hydrometric and sedimentary data is from the Nwanedi Dam catchment in South Africa (Figs. 2–3). Hydrometric data from Ripple Creek Dam, Massingir Dam and Shashe Dam are combined with sedimentary proxies in Figs. 4, 5 and 6. In order to identify the general trends of river flows during major rainy events, the discharge data along the Limpopo River tributaries in Botswana (Metsimotlhabe, Mahalapye, Lotsane, Shashe and Motloutse rivers), South Africa (Oliphant, Lephalale, Crocodile, Sand and Luvuvhu rivers), Zimbabwe (Shashe, Mzingwane and Mwenezi rivers) were analysed (S.O.M. 1). The cross referencing of river discharge values with the daily rain events exceeding the 99th percentile and dam level fluctuations pinpointed 19 potential flood events in South Africa, Zimbabwe, Mozambique and Botswana between 1977 and 2017 (Table 1; S.O.M. 1). The most severe flood events reported in the literature for the same time period occurred in 1996/97 and 1999/2000 (Trambauer et al., 2015) and 2013 (Spaliviero et al., 2014; Manhique et al., 2015). This iterative analysis of the available data sets identified 6 major flood events that occurred in the LRB during 1988–89, 1995–96, 1999–00, 2003–04, 2010–11, 2013–14 and 2016–17 (Table 1).

The individual flood events preserved in the cores were identified by analysing the sediment grain-size distributions with the End Members Modelling Analysis (EMMA) algorithm of Hartmann et al. (2023). The method presented in Weltje and Prins (2007) was applied to the estimate of flood magnitudes as in Toonen et al. (2015) and Munoz et al. (2018). Previous studies have demonstrated that the coarser end-members (EM) correlate well with river discharge in the basin and are therefore reliable proxies for inferring the flood magnitude (Toonen et al., 2015). During a flood, the competence of the river increases and larger amounts of coarser grains are entrained in the suspended load and finally trapped in the dams as flood couplets (e.g., Toonen et al., 2015; Franchi et al., 2020). The EMMA is used to identify the coarse tail of grain size distribution of flood couplets that, in turn, can identify the peak discharge magnitude. The two EM from the coarse tail of the sediment distribution were compared with known discharge rates from gauging stations and other hydrometeorological data and used to pinpoint the sedimentary flood events. Summary of the sedimentary floods events are presented in Figs. 2 to 6.

3.2. Prolonged droughts periods in the LRB

Droughts were identified by cross referencing annual (12 months' time scale) climatological drought indices (Standardized Precipitation Index – SPI and Standardized Precipitation Evapotranspiration Index - SPEI) with available meteorological data from observation records, literature and reports (Table 1). Drought years were further identified through a variable threshold analysis of the discharge data, identifying the thresholds according to a percentile of 0.80 (Table 1). Hydrological droughts are reported in literature in 1979 (Schulze, 1984), in 1982–83 (groundwater drought; Schulze, 1984), in 1984 (only in Botswana), 1986–87, 1991–92 (groundwater drought), 1994–95, 2002–03, 2005–06 (Wessels et al., 2004; Trambauer et al., 2015) showing significant spatial variability, with 1991–92 drought being the most severe of the last 50 years (Wessels et al., 2004; Trambauer et al., 2015). More recently, the basin recorded droughts in 2010 and 2015–16 (Table 1).

The SPI and SPEI results for Nwanedi Dam are reported in Fig. 3, confirming the severe droughts of 1991–92, 1994–95 and 2002–03. Annual SPI for Ripple Creek, Massingir, and Shashe dam catchments are shown in Figs. 4, 5 and 6, respectively. Moderate (SPI = −1.00 to −1.49) to severe (SPI = −1.50 to −1.99) meteorological droughts are recurrent in the basin (Table 1). Extreme droughts (SPI = −2.00 or less) have been observed in Ripple Creek Dam, Shashe Dam and Massingir Dam in 1982–83, 1991–92 and 2002–03 (Figs. 4–6). The extreme event of 1991 was protracted for >3 hydrological years in the Shashe Dam sub-basin. There is no visible increasing or decreasing trend for drought occurrence

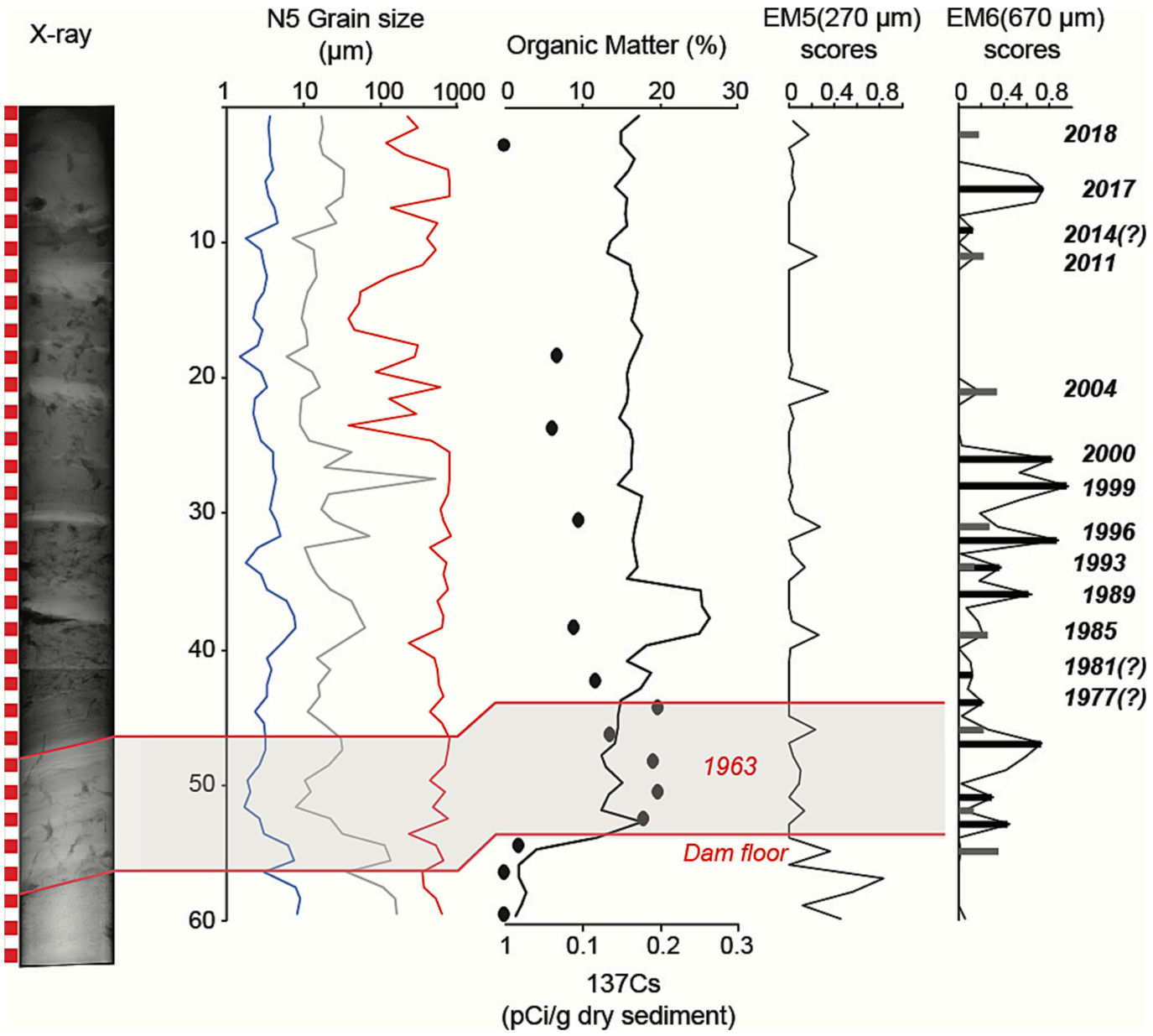

Fig. 2. Sediments core from the Nwanedi Dam (from left to right): x-ray image of the core N5; grain size distribution Dx10 (blue), Dx50 (grey) Dx90 (red); Organic matter content and ^{137}Cs activity (solid black circles); End Member scores for EM5 (270 μm) and EM6 (670 μm). EM5 is in grey in the last column on the right while EM6 values are in black.

as defined by SPI calculations. Nevertheless, the drought frequency and intensity are both increasing in a downstream direction (e.g., from Shashe to Massingir dams).

4. Discussion

4.1. What are the processes that influence the severity and frequency of floods in the LRB?

In Southern Africa, negative ENSO events (La Niña) lead to above-average precipitations while positive ENSO events (El Niño) lead to below-average precipitations (Sorensen et al., 2021; Malherbe et al., 2014). However, the relationship between the intensity of ENSO events and rainfall in the Limpopo River Basin is non-linear, because the South Indian Ocean Dipole (SIOD) and the Southern Annular Mode (SAM) also play an important role in rainfall generation (Rapolaki et al., 2019).

During the moderate/strong El Niño years in 1982–83, 1986–88, 1991–92, 1994–95, 1997–98, 2002–03, and 2015–16, drought conditions were recorded in the LRB whereas the moderate El Niño conditions in 2009–10 did not cause droughts (Table 1; Figs. 3–6). The observed drought conditions were then followed by heavy rainfall in 1985, 1989, 1996, 2000 and 2017, which in 4 cases out of 5 resulted in devastating floods (Table 1). However, there are no systematic correlation between these extreme floods and ENSO across the basin. In the less arid parts of the basin (i.e. mostly Mozambique and South Africa), the magnitude of floods was found to be correlated with antecedent prolonged drier-than-usual periods (Fig. 7). Specifically, for the Nwanedi and Massingir dam catchments, the comparison of river flow data and SPI (over the hydrological year July–June) shows a strong positive correlation (Fig. 7), meaning that over 75 % of variability in flow can be explained by SPI. More interestingly, the correlation was found to be strongly negative ($R^2 = 0.79$) between maximum annual flow and the SPI of the previous 4 years (in phase with ENSO). These results suggest that in the less arid parts of the basin, drier-than-normal antecedent conditions, including

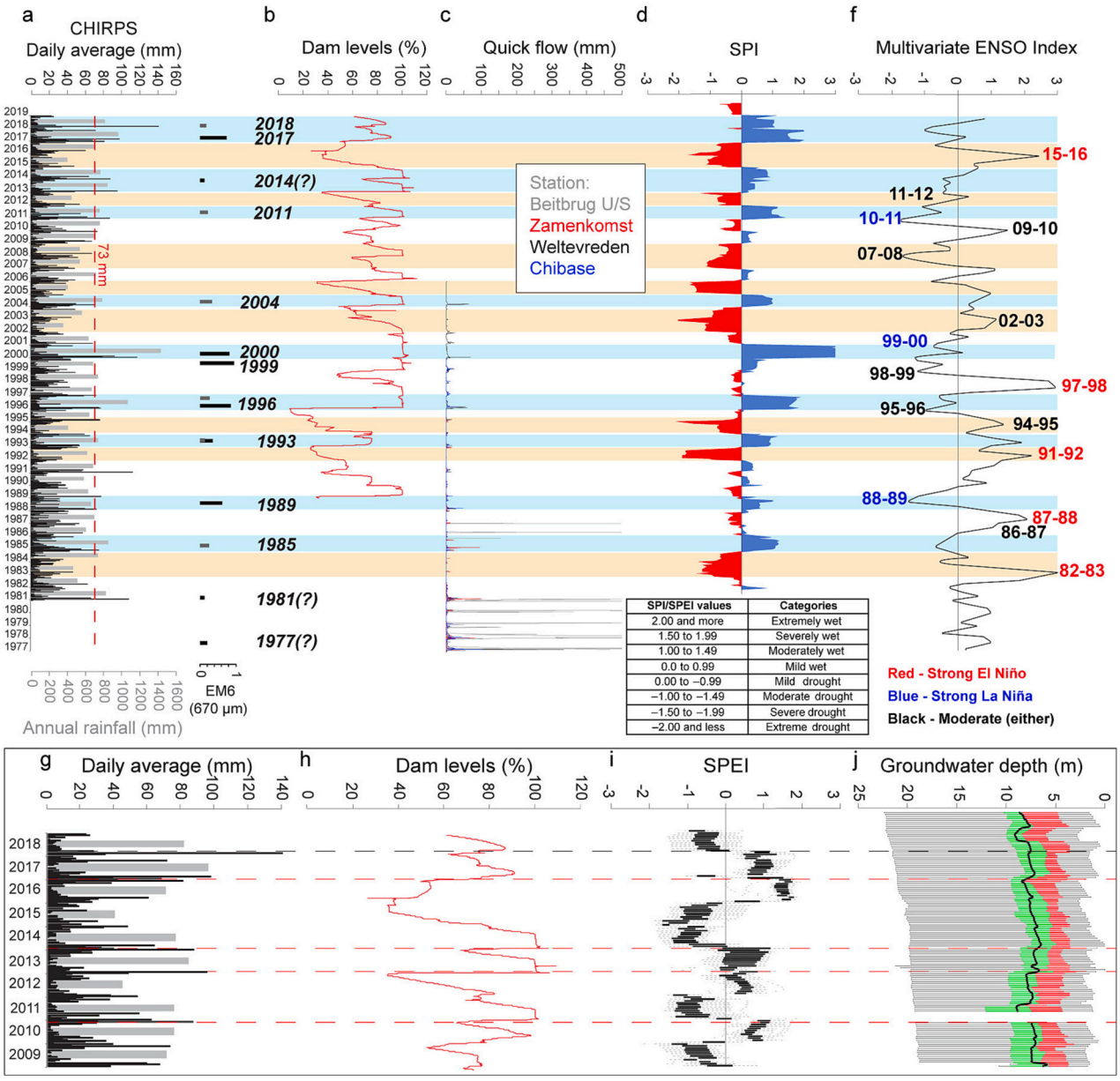

Fig. 3. Sedimentological and hydrological data from Nwanedi dam catchment. Upper panel: a) CHIRPS rainfall data across the Nwanedi dam catchment; Results of the EMMA analysis, EM6 values are presented in black while EM5 are in grey; b) Nwanedi Dam levels; c) quick flow measurements for 4 GRDC stations (see Fig. 1 for locations): Chibase (1196310) and Weltevreden (1196330) = Luvuvhu River; Zamenkomst (1196500) = Sand River; Beitbrug U/S (1196550) = Limpopo River; d) Standardized Precipitation Index (SPI) at the timescales of 12 months for Nwanedi, red areas represent droughts, and blue areas represents wetter periods; f) multivariate ENSO indexes from Baddoo et al. (2015).
In this panel the main droughts are highlighted in light orange while the major flood events are highlighted in blues; droughts and floods are identified using all available data sets as in Table 1 and S.O.M. 1.
Lower panel: g) CHIRPS rainfall data across the Nwanedi dam catchment between 2009 and 2019; h) Nwanedi Dam levels between 2009 and 2019; i) Standardized Precipitation Evapotranspiration Index (SPEI) at the timescales of 12 months for Nwanedi Dam, the variation across the basin is presented by the box pot; j) monthly groundwater depth (box plots), including average level (black thick line), red bars are the 25th percentile, green bars are the 75th percentile.

major, prolonged droughts, increase susceptibility to major floods once wetter-than-normal conditions are met (i.e., heavy rains).

In contrast, river flow data and SPI do not show any meaningful correlation in the Shashe and Ripple Creek dam catchments, both located in more arid parts of the LRB (Fig. 7). Therefore, in the more arid parts of the basin, which are already affected by relatively dry conditions even during wetter-than-normal ENSO, drier-than-normal antecedent conditions do not seem to increase susceptibility to intense floods. This dichotomy can be explained by a range of physical factors that characterize the less vs more arid regions of the LRB such as, for the latter, scarce vegetation and drier, already deteriorated soils, different geological substrates, and deeper water tables, altogether implying prevailing ubiquitous dry conditions and therefore low vulnerability to severe droughts (Fig. 1B).

Mathivha et al. (2016), presented deteriorating land cover conditions in the Luvhuvhu River catchment (adjacent to the Nwanedi dam's catchment) coupled with a flood volume increase of 11 % between 1963 and 2013. The authors did not link changes in land cover with increasing negative effects of droughts in the region but nevertheless recommended preservation of natural forests and sustainable agriculture. The 1999 National Review of Land Degradation includes the area of the Nwanedi Dam as affected by severe soil degradation (Hoffman and Todd, 2000;

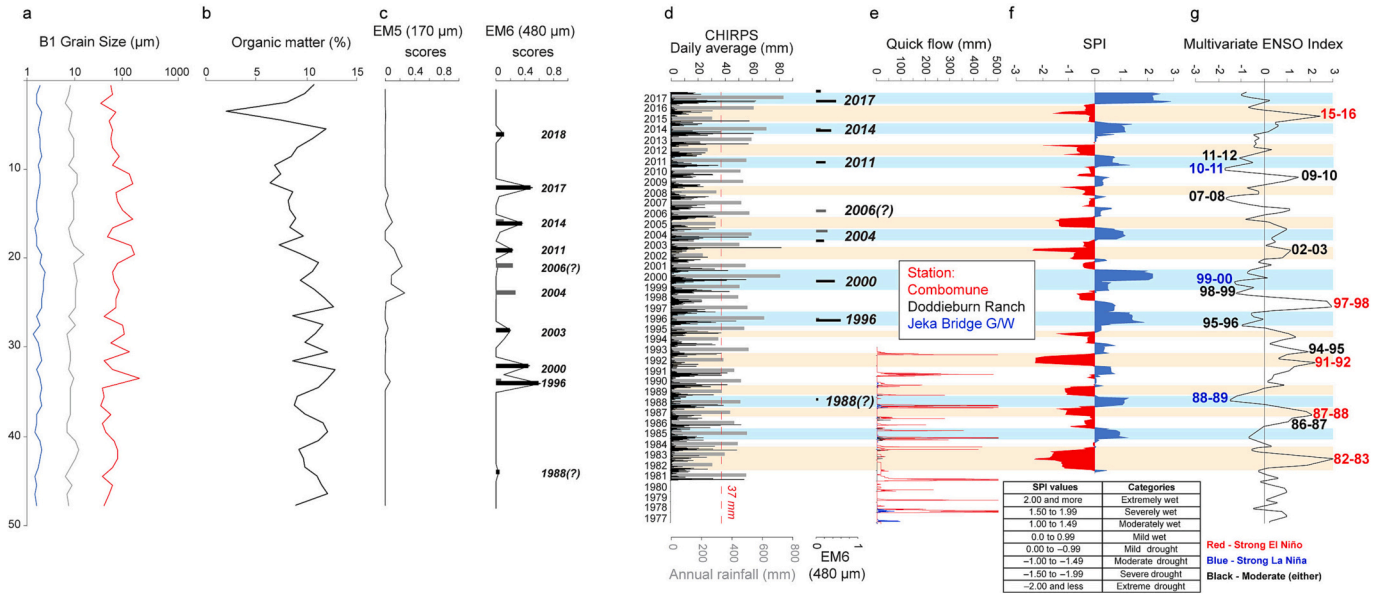

Fig. 4. Sedimentological and hydrological data from Ripple Creek Dam catchment a) grain size distribution Dx10 (blue), Dx50 (grey) Dx90 (red) of sediments core B1 from the Ripple Creek Dam; b) Organic matter content of core B1; c) End Member scores for EM5 (170 μm) and EM6 (480 μm); d) CHIRPS rainfall data across the Ripple Creek Dam catchment and EMMAgeo results for EM6 (in black); e) quick flow measurements for 3 GRDC stations (see Fig. 1 for locations): Jeka Bridge G/W (1496360) = Mwenezi River; Doddieburn Ranch (1496321) = Mzingwane River; Combomune (1896502) = Limpopo River; f) Standardized Precipitation Index (SPI) at the timescales of 12 months for Massingir Dam, red areas represent droughts, and blue areas represents wetter periods; g) multivariate ENSO indexes from Baddoo et al. (2015).
In this panel the main droughts are highlighted in light orange while the major flood events are highlighted in blues; droughts and floods are identified using all available data sets as in Table 1 and S.O.M. 1.

Wessels et al., 2004). The authors further indicated that the relative impact of degradation was most pronounced during the dry periods and that "desertification" in Africa could be primarily attributed to droughts (Wessels et al., 2004 and references therein). From the available studies for the region it can be deduced that human-induced land degradation most likely alters the vegetation cover and function increasing the extent of soil erosion (e.g. Wessels et al., 2004).

Several studies concluded that soil deterioration and loss of vegetation during periods of drought could explain the increased magnitude (and possibly areal extent) of flood events after drought (Dunbar et al., 2010; Franchi et al., 2020). Recent modelling by Kim et al. (2023), despite limited by a lack of in situ data in Mozambique, Botswana, and Zimbabwe, revealed a positive correlation between precipitation and vegetation health although they found no clear trend in the changes of vegetation across the LRB. The authors point out that the Normalized Difference Vegetation Index (NDVI) can vary across the LRB due to variability of geological characteristics (i.e. deeper aquifers in crystalline basement vs shallower aquifers in the alluvium) and climatic conditions (i.e., more arid in the upper LRB and more humid in the lower reaches of the LRB). It appears as if, at the basin scale, the vegetation in the LRB can withstand prolonged drought events (Kim et al., 2023). But there are still no unambiguous data revealing the changes of vegetation and soils at the sub-basin scale. The loss of vegetation during prolonged dry periods coupled with soil crusting and compaction during droughts can cause an increase of runoff, especially in the most arid part of the basin (Descroix et al., 2009). Increase of runoff and soil deterioration might in turn increase erosion and hence the volume of sediments transported by floods resulting in thicker and coarser flood sediments layers. The EMMA analysis would therefore consider these events of higher magnitude with respect of floods occurring over a less deteriorated basin.

The study of the sedimentary records augments data availability, both spatially and temporally, in poorly gauged river systems, allowing for a regional comparison of changing flood dynamics in response to climate and human impacts (e.g., Wirth et al., 2013). In general terms, the magnitude of sedimentary floods depends on the river discharge but large floods are linked to a range of rainfall conditions, rather than systematic high intensity events, as larger events can occur either after drought or over saturated systems due to multiple years of abundant rains. Nevertheless, it is clear that the use of rainfall series alone cannot explain the occurrence and magnitude of flood events in a large arid to semi-arid river basin like the LRB. The link between rainfall intensity and flooding events is non-linear, generally, as the magnitude of floods is often decoupled from the magnitude of extreme rainfall events (e.g. Nwanedi Dam; Fig. 3).

In conclusion, it appears that the severity and frequency of extreme flood events is driven by extreme weather events, soils deterioration, vegetation loss, depth to water table and geological conditions. Further studies should assess the respective importance of each of these factors through downscaling the analysis to smaller sub-catchments.

4.2. *The interlink between groundwater levels and floods in the LRB*

An additional process to consider is the interaction between groundwater and surface water during extreme hydrological events. In this study, we explored the link between groundwater table levels and severity of floods. For this preliminary analysis, we used the recorded time series of water table changes in the Nwanedi Dam basin and compared it with SPEI values (inset in Fig. 3). At the temporal scale of individual flood-drought cycles (considered as flood and drought events that occur in succession), the groundwater table drops during droughts – or in normal years, during the dry season and the first half of the rain season – only to suddenly rise during and after the floods (Fig. 3). For instance, in correspondence of the flood events of 2011, 2013, 2014 and 2017 the groundwater table shows an abrupt increase followed by a gradual decrease, which is a typical response to groundwater recharge. As flood events in the LRB are increasing in frequency and magnitude, we would expect an overall increase in groundwater recharge and hence, an increasing water table. However, the available groundwater level data show an overall continuous water table decline (bold black

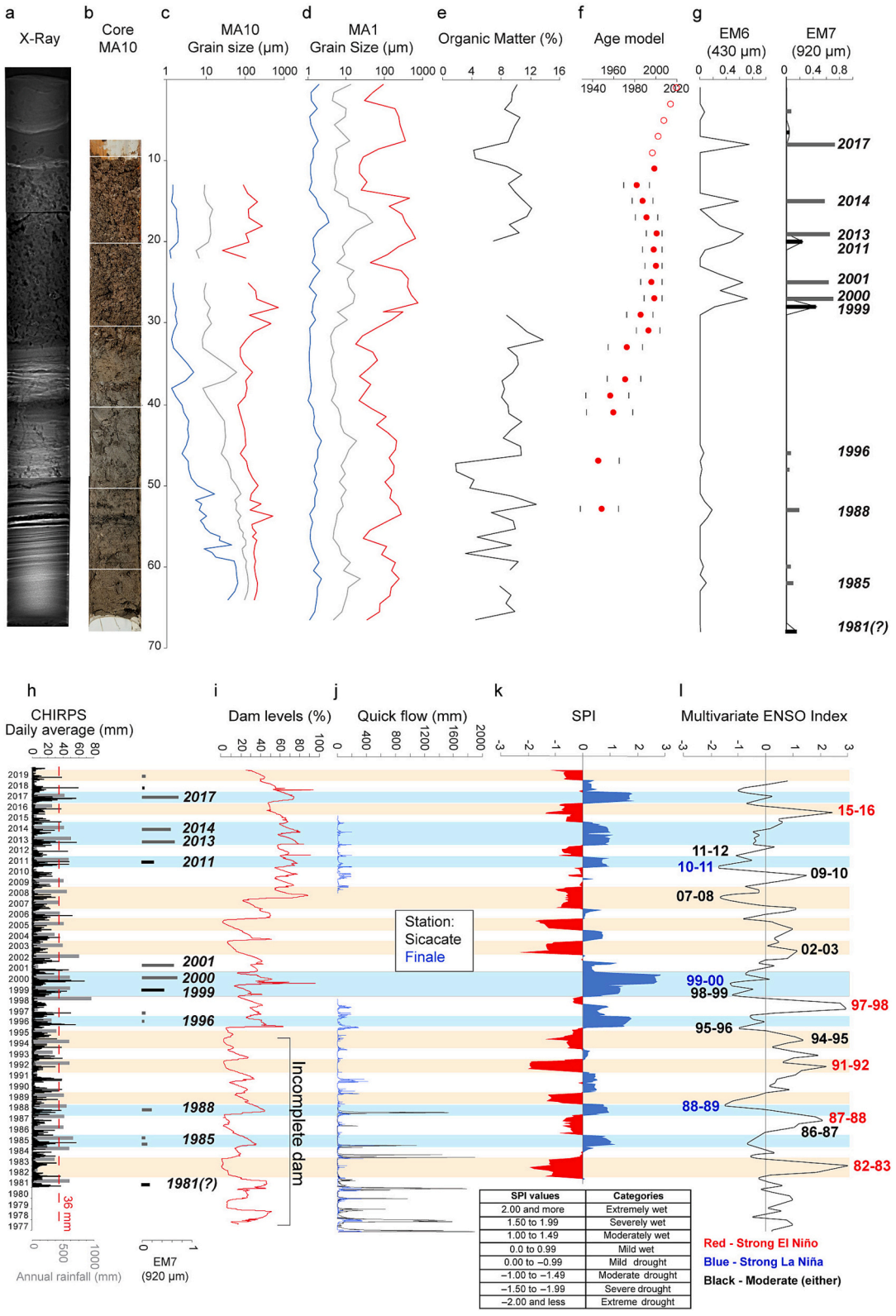

Fig. 5. Sedimentological and hydrological data from Massingir Dam catchment. a) x-ray image of the core MA10; b) photograph of the core MA10; c) grain size distribution Dx10 (blue), Dx50 (grey) Dx90 (red) of the core MA10; d) grain size distribution Dx10 (blue), Dx50 (grey) Dx90 (red) of the core MA1; e) organic matter content of the core MA1; f) age model of the core MA1, the age model is based on ^{210}Pb dating method using the constant initial concentration dating model; g) End Member scores for EM6 (430 μm) and EM7 (920 μm) for core MA1; in the last column on the right EM6 are plotted in grey and EM7 are plotted in black. h) CHIRPS rainfall data across the Massingir Dam catchment and results of the EMMAgeo EM7; i) Massingir Dam levels; j) quick flow measurements for 2 GRDC stations (see Fig. 1 for locations): Finale (1196100) = Oliphant River; Sicacate (1896501) = Limpopo River; k) Standardized Precipitation Index (SPI) at the timescales of 12 months, red areas represent droughts, and blue areas represents wetter periods; l) multivariate ENSO indexes from Baddoo et al. (2015).
In this panel the main droughts are highlighted in light orange while the major flood events are highlighted in blues; droughts and floods are identified using all available data sets as in Table 1 and S.O.M. 1.

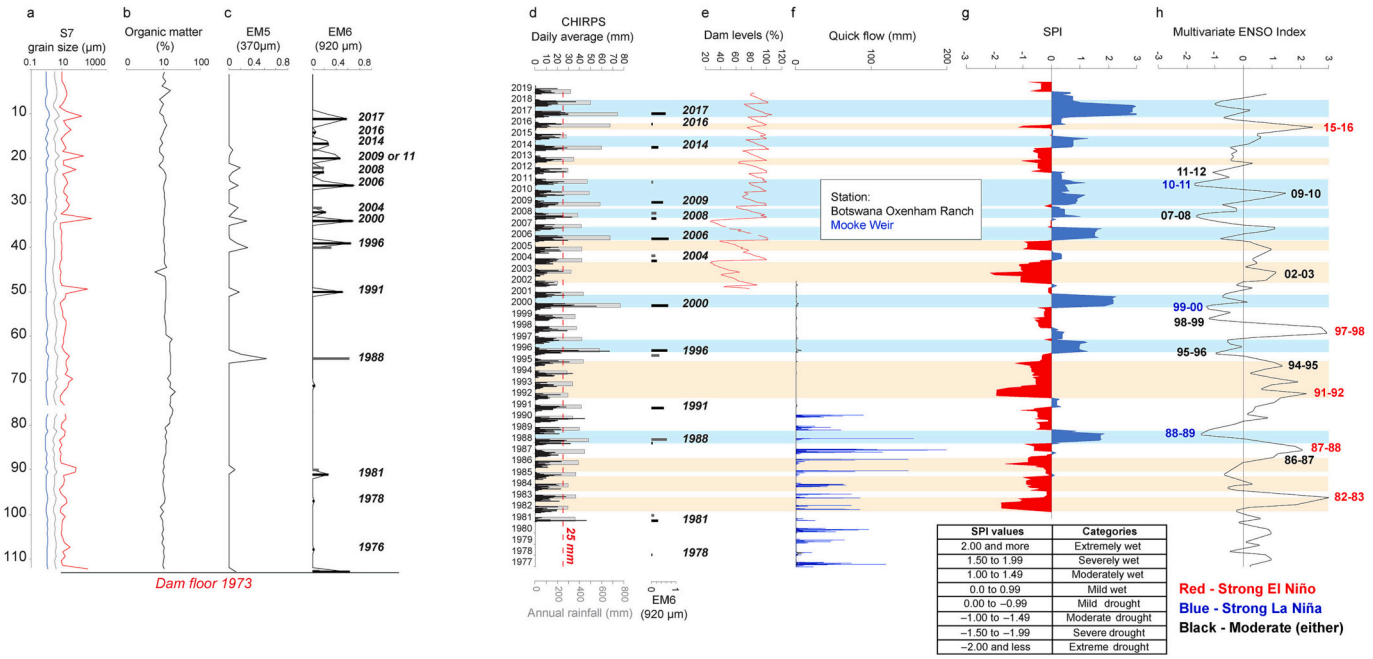

Fig. 6. Sedimentological and hydrological data from Shashe Dam catchment. a) grain size distribution Dx10 (blue), Dx50 (grey) Dx90 (red) of sediments core S7; b) organic matter content of sediments core S7; c) End Member scores for EM5 (370 μm) and EM6 (920 μm), in the last column on the right EM5 values are plotted in grey while EM6 values are plotted in black; d) CHIRPS rainfall data across the Shashe Dam catchment; e) Shashe Dam levels; f) quick flow measurements for 2 GRDC stations (see Fig. 1 for locations): Mooke Weir (1396010) = Shashe River; Botswana Oxenham Ranch (1196400) = Limpopo River; g) Standardized Precipitation Index (SPI) at the timescales of 12 months, red areas represent droughts, and blue areas represents wetter periods; h) multivariate ENSO indexes from Baddoo et al. (2015).
In this panel the main droughts are highlighted in light orange while the major flood events are highlighted in blues; droughts and floods are identified using all available data sets as in Table 1 and S.O.M. 1.

line in the inset of Fig. 3), which would indicate that either (1) locally increasing recharge associated with more frequent and intense floods does not compensate for a long-term regionally decreasing recharge associated with increase of the duration and intensity of drought events, whereby minor recharge events typically associated with moderate rainfall events across the basin have become less frequent or (2) that increasing groundwater abstraction rates across the basin, as a result of population growth and increasing surface water scarcity associated to droughts, outweigh the increased recharge (Masiyandima et al., 2002; Busari, 2008; Abiye et al., 2020; Sorensen et al., 2021), or a combination of both. More continue data sets, unavailable in the rest of the LRB, would be necessary to study this trend.

4.3. The role of groundwater-surface water relationships across the LRB on the impact of hydroclimatic events

The results of the EMMAGeo analysis, SPI, and the river discharge analyses (maximum flow, average flow and POT) unveil a possible scenario concerning the links between drought and flood events. In particular, increased soil compaction during prolonged drought conditions (4 years) may have led to decreasing soil infiltration capacity (Descroix et al., 2009). This, added to the loss of vegetation, may have increased runoff coefficient explaining the occurrence of flood events after prolonged drought conditions. This is likely to be the case for most of the lower and middle reaches of the LRB, which are characterized by less arid conditions, and show meaningful correlation between higher river flows and concurrent wetter-than-normal conditions immediately following prolonged drier-than-normal conditions (Fig. 7). It is thought that, in this scenario, soil degradation and increasing groundwater abstraction – the latter causing long-term decline of groundwater levels (inset in Fig. 3) – have reduced surface water-groundwater interactions, which in turn amplifies surface droughts through reduced river baseflow; especially in low-lands and floodplains where the water table is shallower as is the case of the lower reaches of the LRB.

In the Shashe and Ripple Creek sub-basins, in the most arid parts of the basin, however, high river flows do not correlate with SPI values, likely because in these arid areas, water tables are much deeper, vegetation is scarce and soils are in a near-permanent dry state regardless of ENSO conditions. This is still a hypothesis and needs more work to be unambiguously proven.

The preliminary analysis on a limited data set available, show that antecedent conditions with exceptionally high groundwater table due to unusually long negative ENSO period (e.g. for the 2013–14 flood events) might also exacerbate floods (Fig. 3). This rise in water table is typical of endorheic areas where rains create persistent ponds and lakes when the water table reaches the surface, such as commonly found in the lower reach of the LRB, in Mozambique.

The data analysed here therefore revealed contrasting scenarios for the upper and lower reaches of the LRB (Fig. 7). This dichotomy, which was primarily explained by the general NW-SE aridity gradient, is likely enhanced by geological variability. Overall, crystalline terrains, which dominate large part of the LRB in Botswana, Zimbabwe and most of northern South Africa (Fig. 1B), are characterized by overall lower permeability bedrock and deeper water table, and as a result river discharge is predominantly supported by surface runoff during high rainfall events (Descroix et al., 2009; Geris et al., 2022). These areas were also reported in Spaliviero et al. (2014) as flood-prone areas during major rainfalls events. In Mozambique, on the other hand, where connectivity between groundwater and surface water prevails, because the water table is shallower and sedimentary terrains have higher groundwater storage, the contribution of groundwater to river discharge is higher (Descroix et al., 2009) (Fig. 1B).

5. Conclusions

This study has identified trends of increasing severity and frequency

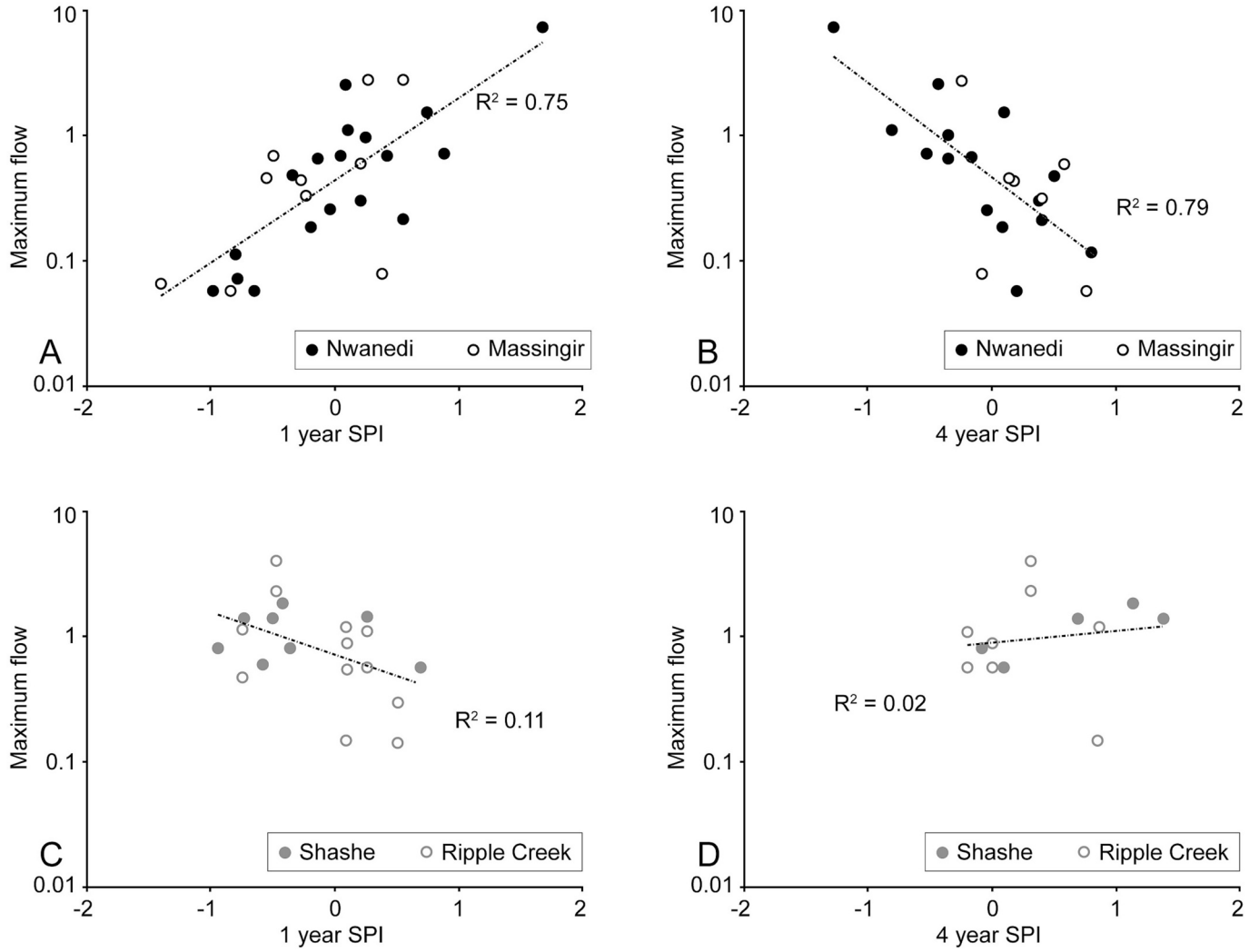

Fig. 7. Statistical analysis of the river flow data and SPI values. A–B) In the two less arid catchments (Nwanedi and Massingir) there are strong exponential correlations between maximum river flow and SPI ($R^2 > 0.75$). The correlation is positive for same year SPI (floods are exponentially more intense when short term conditions are wetter than normal) and negative for previous 4 years SPI (floods are exponentially more intense when long term antecedent conditions are drier than normal). C–D) In the two more arid catchments (Shashe and Massingir) there is a weak negative correlation between maximum flow and same year SPI ($R^2 = 0.11$), suggesting to small extent that floods intensity is sometime related to drier concurrent conditions, regardless of long term antecedent conditions since there is no meaningful correlation between maximum flow and 4 years SPI.

of flood events in the LRB that show apparent correlations with an increasing severity of droughts (positive ENSO events) and, for the last decade, with an overall long-term decline in groundwater levels (Fig. 3). The links between drier-than-usual periods and maximum river flows is clear in the less arid region of the LRB. There, intense floods correlate with wetter than normal periods (i.e., an 'activation' period) immediately following intense prolonged droughts. In the more arid regions of the LRB, the limited data available hampered our ability to identify significant correlations, urging for an improvement and expansion of monitoring infrastructure.

Over the last 40 years, climate and land use changes have impacted river flow regimes in the LRB and modified the natural interannual oscillation linked to ENSO causing devastating and unpredictable flood events, often following prolonged dry periods. Existing climate projections for parts of the LRB consider the impact of changing climate and forecast a higher proportion of dry years in the next century, which will translate into more frequent droughts and soils degradation and, therefore, potentially more devastating floods.

The proposed approach using supplementary data from flood sediment records can be used to constrain potential environmental scenarios that can be analysed in advance, allowing for the identification of appropriate management solutions to improve resilience to hydrological extremes in data scarce developing countries' semi-arid river basins. Further separation of respective contribution of long-term drought, human activity and geological heterogeneity requires downscaling the approach individual smaller catchment which we recommend as part of future research.

Supplementary data to this article can be found online at https://doi.org/10.1016/j.scitotenv.2024.171489 (Franchi et al., 2023).

CRediT authorship contribution statement

Fulvio Franchi: Writing – review & editing, Writing – original draft, Investigation, Formal analysis, Data curation, Conceptualization. **Syed Mustafa:** Writing – review & editing, Methodology, Data curation. **Daniel Ariztegui:** Writing – review & editing, Funding acquisition. **Farisse J. Chirindja:** Investigation. **Andrea Di Capua:** Writing – review & editing, Visualization. **Stephen Hussey:** Investigation. **Jean-Luc Loizeau:** Writing – review & editing, Formal analysis, Data curation. **Vittorio Maselli:** Writing – review & editing, Data curation. **Alessia Matanó:** Writing – review & editing, Methodology, Formal analysis, Data curation. **Oluwaseun Olabode:** Methodology, Formal analysis,

Data curation. **Florian Pasqualotto:** Visualization, Investigation, Formal analysis. **Whatmore Sengwei:** Writing – review & editing, Visualization, Methodology, Formal analysis. **Sithabile Tirivarombo:** Writing – review & editing. **Anne F. Van Loon:** Writing – review & editing, Methodology, Data curation. **Jean-Christophe Comte:** Writing – original draft, Methodology, Funding acquisition, Conceptualization, Data curation.

Declaration of competing interest

There are no conflict of interest to report in this work, nor known competing financial interests.

Data availability

Data will be made available on request.

Acknowledgements

The authors would like to extend their warmest gratitude to Mr. Kaene Abidile and Mr. Lesego Raditsebe from WUC of Botswana for dam levels and other important data and for the assistance with the permits for the sampling activities in Botswana; to Mr. Nhlapo Elias and Mr. Majola Kwazikwakhe from DWS South Africa for the Nwanedi dam levels and to Mr. Wilson Nkuna for the assistance with the permits to visit the dams in South Africa; Mr. Shephard Shumba and Mr. Farai Manzira from ZIMWA for the dam levels and other important data from Zimbabwe and for the assistance with the permits; Ms. Lizete Dias from ARA-Sul and Dr. Agostinho Vilanculos from DNGRH (National Directorate of Water Resources Management) for the Massingir Dam levels. Thanks are due to Gizaw Mengistu (BIUST) for the assistance with the CHIRPS data set. To Mr. Omogolo Keobokile (BIUST/Copperbelt University) and Ms. Rorisang Tisane goes our gratitude for the invaluable help during the collection and preparation of samples and for the sedimentological analyses of the samples from Botswana and Mozambique. This work is dedicated to the memory of Pardington Mukombwe, prematurely passed after graduation at the University of Zimbabwe, he worked with passion in the field and keen interest in the lab, you will be missed.

This work was undertaken as part of the project CONNECT4 Water Resilience project funded by the UK Natural Environment Research Council (NERC) and the UK Foreign, Commonwealth & Development Office (FCDO) under the Science for Humanitarian Emergencies and Resilience (SHEAR) programme (grant number NE/S005943/1).

References

Abiye, T.A., Tshipala, D., Leketa, K., Villholth, K., Magombeyi, M., Ebrahim, G., Butler, M., 2020. Hydrogeological characterization of crystalline aquifer in the Hout River catchment, Limpopo province. South Africa Groundwater for Sustainable Development 100406. Groundw. Sustain. Dev. 11, 100406.

Alemaw, B.F., Kileshye-Onema, J.M., Love, D., 2013. Regional drought severity assessment at a basin scale in the Limpopo drainage system. J. Water Resource Prot. 5, 1110–1116.

Appleby, P.G., 2001. Chronostratigraphic techniques in recent sediments. In: Last, W.M., Smol, J.P. (Eds.), Tracking Environmental Change Using Lake Sediments, Basin Analysis, Coring and Chronological Techniques, vol. 1. Kluwer Academic Publishers, Dordrecht, pp. 171–203.

Baddoo, T.D., Guan, Y., Zhang, D., Andam-Akorful, S.A., 2015. Rainfall variability in the Huangfuchuang watershed and its relationship with ENSO. Water 7, 3243–3262.

Barton, J.M., Zeh, A., Klemd, R., 2006. The Limpopo Belt: a result of Archean to Proterozoic, Turkic-type orogenesis?. In: Special Paper of the Geological Society of America, vol. 405, pp. 315–332.

Booth, D.B., Henshaw, P.C., 2001. Rates of channel erosion in small streams. In: American Geophysical Union. Land Use and Watersheds: Human Influence on Hydrology and Geomorphology in Urban and Forest Areas, vol. 2, pp. 17–38.

Botai, C.M., Botai, J.O., Zwane, N.N., Hayombe, P., Wamiti, E.K., Makgoale, T., et al., 2020. Hydroclimatic extremes in the Limpopo River Basin, South Africa, under changing climate. Water 12, 3299.

Bumby, A.J., Eriksson, P.G., Catuneanu, O., Nelson, D.R., Rigby, M.J., 2012. Meso-archaean and palaeo-proterozoic sedimentary sequence stratigraphy of the Kaapvaal Craton. Mar. Pet. Geol. 33, 92–116.

Busari, O., 2008. Groundwater in the Limpopo Basin: occurrence, use and impact. Environ. Dev. Sustain. 10, 943–957.

Carleton, T.A., Hsiang, S.M., 2016. Social and economic impacts of climate. Science 353, 6304.

Catuneanu, O., Wopfner, H., Eriksson, P.G., Cairncross, B., Rubidge, B.S., Smith, R.M.H., Hancox, P.J., 2005. The Karoo basins of south-central Africa. J. Afr. Earth Sci. 43, 211–253.

Coppus, R., Imeson, A.C., 2002. Extreme events controlling erosion and sediment transport in a semi-arid sub-andean valley. Earth Surf. Process. Landforms 27, 1365–1375.

Descroix, L., Mahé, G., Lebel, T., Favreau, G., Galle, S., Gautier, E., Olivry, J.-C., Albergel, J., Amogu, O., Cappelaere, B., Dessouassi, R., Diedhiou, A., Le Breton, E., Mamadou, I., Sighomnou, D., 2009. Spatio-temporal variability of hydrological regimes around the boundaries between Sahelian and Sudanian areas of West Africa: a synthesis. J. Hydrol. 375, 90–102.

Devitt, L., Neal, J., Wagener, T., Coxon, G., 2021. Uncertainty in the extreme flood magnitude estimates of large-scale flood hazard models. Environ. Res. Lett. 16, 064013.

Dietze, E., Hartmann, K., Diekmann, B., Ijmker, J., Lehmkuhl, F., Opitz, S., Stauch, G., Wünnemann, B., Borchers, A., 2012. An end-member algorithm for deciphering modern detrital processes from lake sediments of Lake Donggi Cona, NE Tibetan Plateau, China. Sediment. Geol. 243–244, 169–180. https://doi.org/10.1016/j.sedgeo.2011.09.014.

Dunbar, J.A., Allen, P.M., Bennett, S.J., 2010. Effect of multiyear drought on upland sediment yield and subsequent impacts on flood control reservoir storage. Water Resour. Res. 46, W05526.

Easterling, D.R., Meehl, G.A., Parmesan, C., Changnon, S.A., Karl, T.R., Mearns, L.O., 2000. Climate extremes: observations, modelling, and impacts. Science 289, 2068–2074.

Evrard, O., Chaboche, P.-A., Ramon, R., Foucher, A., Laceby, J.P., 2020. A global reviewof sediment source fingerprinting research incorporating fallout radiocesium (^{137}Cs). Geomorphology 362, 107103.

FAO, 2020. WaPOR—the FAO portal to monitor water productivity through open access or remotely sensed derived data, FAO, Rome, Italy. Retrieved from. https://wapor.apps.fao.org/home/1.

Fitchett, J.M., Grab, S.W., 2014. A 66-year tropical cyclone record for south-east Africa: temporal trends in a global context. Int. J. Climatol. 34, 3604–3615. https://doi.org/10.1002/joc.3932.

Foster, I.D.L., Boardman, J., Keay-Bright, J., Meadows, M.E., 2005. Land degradation and sediment dynamics in the South African Karoo. Int. Assoc. Hydrol. Sci. Publ. 292, 207–213.

Franchi, F., Mapeo, R.B.M., 2019. Evolution of an Archean intracratonic basin: a review of the Transvaal Supergroup lithostratigraphy in Botswana. Earth Sci. Rev. 191, 273–290.

Franchi, F., Ahad, J.M.E., Geris, J., Jhowa, G., Petros, A.K., Comte, J.-C., 2020. Modern sediment records of hydroclimatic extremes and associated potential contaminant mobilization in semi-arid environments: lessons learnt from recent flood/drought cycles in Southern Botswana. J. Soils Sediments 20, 1632–1650.

Franchi, F., Chirindja, F.J., Pasqualotto, F., Hussey, S., Comte, J-C., 2023. Sedimentological data from the Limpopo River Basin dams, southern Africa, 2018-2021. NERC EDS Environmental Information Data Centre (Dataset). https://doi.org/10.5285/b8db8239-3bde-454a-aa75-d1cec24c8763.

Funk, C., Peterson, P., Landsfeld, M., Pedreros, D., Verdin, J., Shukla, S., Husak, G., Rowland, J., Harrison, L., Hoell, A., Michaelsen, J., 2015. The climate hazards infrared precipitation with stations—a new environmental record for monitoring extremes. Sci. Data 2, 1–21.

Geris, J., Comte, J.-C., Franchi, F., Petros, A.K., Tirivarombo, S., Selepeng, A.T., Villholth, K.G., 2022. Surface water-groundwater interactions and local land use control water quality impacts of extreme rainfall and flooding in a vulnerable semi-arid region of Sub-Saharan Africa. J. Hydrol. 609, 127834.

Goode, J.R., Luce, C.H., Buffington, J.M., 2012. Enhanced sediment delivery in a changing climate in semi-arid mountain basins: Implications for water resource management and aquatic habitat in the northern Rocky Mountains. Geomorphology 139, 1–15.

Haimann, M., Liedermann, M., Lalk, P., Habersack, H., 2014. An integrated suspended sediment transport monitoring and analysis concept. Int. J. Sediment Res. 29 (2014), 135–148.

Hamlet, A.F., Lettenmaier, D.P., 2007. Effects of 20th century warming and climate variability on flood risk in the western U.S. Water Resour. Res. 43, W06427.

Hartmann, K., Krois, J., Rudolph, A., 2023. Statistics and Geodata Analysis using R (SOGA-R). Department of Earth Sciences, Freie Universitaet Berlin. https://www.geo.fu-berlin.de/en/v/soga-r/Advances-statistics/Multivariate-approaches/Factor-Analysis/End-member-modelling-analysis/The-EMMA-algorithm/index.html.

He, Q., Walling, D., 1996. Interpreting particle size effects in the adsorption of ^{137}Cs and unsupported ^{210}Pb by mineral soils and sediments. J. Environ. Radioact. 30, 117–137.

Hoffman, M.T., Todd, S., 2000. A National Review of land degradation in South Africa: the influence of biophysical and socio-economic factors. J. South. Afr. Stud. 26 (4), 743–758. https://doi.org/10.1080/713683611.

Key, R.M., Ayers, N., 2000. The 1998 edition of the National Map of Botswana. In: Mapeo, R.B.M., Delvaux, D., Kampunzu, A.B., Wendorff, M. (Eds.), Journal of African Earth Sciences, vol. 30, pp. 427–451.

Kim, K.Y., Scanlon, T., Bakar, S., Lakshmi, V., 2023. Decoupling of ecological and hydrological drought conditions in the Limpopo River Basin inferred from groundwater storage and NDVI anomalies. Hydrology 10, 170. https://doi.org/10.3390/hydrology10080170.

Lang, M., Ouarda, T.B.M.J., Bobée, B., 1999. Towards operational guidelines for over-threshold modeling. J. Hydrol. 225, 103–117.
Limpopo Basin Permanent Technical Committee, 2010. Joint Limpopo River Basin study scoping phase final report, República De Moçambique, Ministério Das Obras Publicas E Habitação, Direcção Nacional De Águas. https://dsc.duq.edu/limpopo-reports.
Lindevall, E., 2017. Limpopo River Basin - disaster risk in a changing environment, GRID-Arendal. https://www.grida.no/publications/280.
Lombaard, J., Sikosana, S., van Niekerk, E., 2015. The development of Limpopo water management area north reconciliation strategy. In: Hydrological Analysis. Main Report, vol. 1. Department of Water and Sanitation, Report N. P WMA 01/000/00/02914/3. https://www.dws.gov.za/iwrp/Limpopo/Documents/2016/LNRS_Hydrological%20Analysis%20Report_Volume%201%20Main%20Report_FINAL_20160610.pdf.
Longmore, M.E., 1982. The caesium dating technique and associated applications in Australia. In: Ambrose, W., Duerden, P. (Eds.), Archaeometry: An Australian Perspective. ANU Press, Canberra.
Malherbe, J., Landman, W.A., Engelbrecht, F.A., 2014. The bi-decadal rainfall cycle, Southern Annular Mode and tropical cyclones over the Limpopo River Basin, southern Africa. Clim. Dyn. 42, 3121–3138. https://doi.org/10.1007/s00382-013-2027-y.
Manhique, A.J., Reason, C.J.C., Silinto, B., Zucula, J., Raiva, I., Congolo, F., Mavume, A. F., 2015. Extreme rainfall and floods in southern Africa in January 2013 and associated circulation patterns. Nat. Hazards 77, 679–691. https://doi.org/10.1007/s11069-015-1616-y.
Mapeo, R.B.M., Ramokate, L.V., Armstrong, R.A., Kampunzu, A.B., 2004. U-Pb zircon age of the upper Palapye group (Botswana) and regional implications. J. Afr. Earth Sci. 40, 1–16.
Maposa, D., Cochran, J.J., Lesaoana, M., 2016. Modelling non-stationary annual maximum flood heights in the lower Limpopo River basin of Mozambique. J. Disaster Risk Stud. 8, a185.
Masiyandima, M., Van der Stoep, I., Mwanasawani, T., Pfupajena, S.C., 2002. Groundwater management strategies and their implications on irrigated agriculture: the case of Dendron aquifer in Northern Province, South Africa. Phys. Chem. Earth (Pt A/B/C) 27, 935–940.
Mathivha, F.I., Kundu, P.M., Singo, L.R., 2016. The impacts of land cover change on stream discharges in Luvuvhu River Catchment, Vhembe District, Limpopo Province, South Africa. WIT Trans. Built Environ. 165, 259–270. https://doi.org/10.2495/UW160231.
McKee, T.B., Doesken, N.J., Kleist, J., 1993. The relationship of drought frequency and duration to time scales. In: Proceedings of the 8th Conference on Applied Climatology, vol. 17 (22), pp. 179–183.
Mosase, E., Ahiablame, L., 2018. Rainfall and temperature in the Limpopo River Basin, Southern Africa: means, variations, and trends from 1979 to 2013. Water 10, 364. https://doi.org/10.3390/w10040364.
Munoz, S.E., Giosan, L., Therrell, M.D., Remo, J.W.F., Shen, Z., Sullivan, R.M., Wiman, C., O'Donnell, M., Donnelly, J.P., 2018. Climatic control of Mississippi River flood hazard amplified by river engineering. Nature 556, 95–98.
Nkunzimana, A., Bi, S., Jiang, T., Wu, W., Abro, M.I., 2019. Spatiotemporal variation of rainfall and occurrence of extreme events over Burundi during 1960 to 2010. Arab. J. Geosci. 12, 176.
Owens, P.N., 2020. Soil erosion and sediment dynamics in the Anthropocene: a review of human impacts during a period of rapid global environmental change. J. Soils Sediments 20, 4115–4143. https://doi.org/10.1007/s11368-020-02815-9.
Owens, P.N., Walling, D.E., 1996. Spatial variability of Caesium-137 inventories at reference sites: an example from two contrasting sites in England and Zimbabwe. Appl. Radiat. Isot. 47 (7), 699–707.
Partington, D., Therrien, R., Simmons, C.T., Brunner, P., 2017. Blueprint for a coupled model of sedimentology, hydrology, and hydrogeology in streambeds. Rev. Geophys. 55, 287–309.
Prins, M.A., Postma, G., Weltje, G.J., 2000. Controls on terrigenous sediment supply to the Arabian Sea during the late quaternary: the Makran continental slope. Mar. Geol. 169, 351–371.
Rapolaki, R.S., Reason, C.J.C., 2018. Tropical storm Chedza and associated floods over south-eastern Africa. Nat. Hazards 93, 189–217.
Rapolaki, R.S., Blamey, R.C., Hermes, J.C., Reason, C.J., 2019. A classification of synoptic weather patterns linked to extreme rainfall over the Limpopo River Basin in southern Africa. Clim. Dyn. 53 (3), 2265–2279.
Reason, C.J.C., 2007. Tropical cyclone Dera, the unusual 2000/01 tropical cyclone season in the Southwest Indian Ocean and associated anomalies in southern Africa. Spec. Issue Trop. Cyclones Meteorol. Atmos. Phys. 97, 273–290. https://doi.org/10.1007/s00703-007-0259-2.
Ritchie, J.C., McHenry, J.R., 1973. Determination of fallout ^{137}Cs and naturally occurring gamma-ray emitters in sediments. Int. J. Appl. Radiat. Isot. 24, 575–578.
Rollinson, H.R., Blenkinsop, T.G., 1995. The magmatic, metamorphic and tectonic evolution of the Northern Marginal Zone of the Limpopo Belt in Zimbabwe. J. Geol. Soc. Lond. 152, 65–75.
Ruotoistenmäki, T., 2008. Geophysical maps and petrophysical data of Mozambique. Geol. Surv. Finland Spec. Pap. 48, 65–80.
Schulze, R.E., 1984. Hydrological simulation as a tool for agricultural drought assessment. Water SA 10, 55–62.
Sima, O., Arnold, D., Dovlete, C., 2001. GESPECOR: a versatile tool in gamma-ray spectrometry. J. Radioanal. Nucl. Chem. 248, 359–364.
Sorensen, J.P.R., Davies, J., Ebrahim, G.Y., Lindle, J., Marchant, B.P., Ascott, M.J., Bloomfield, J.P., Cuthbert, M.O., Holland, M., Jensen, K.H., Shamsudduha, M., Villholth, K.G., MacDonald, A.M., Taylor, R.G., 2021. The influence of groundwater abstraction on interpreting climate controls and extreme recharge events from well hydrographs in semi-arid South Africa. Hydrogeol. J. 29, 2773–2787.
Spaliviero, M., De Dapper, M., Maló, S., 2014. Flood analysis of the Limpopo River basin through past evolution reconstruction and a geomorphological approach. Nat. Hazards Earth Syst. Sci. 14, 2027–2039.
Stagman, J.G., 1984. Geological Map of Zimbabwe, 1: 1 000 000 (Reprinted 1994), 7th edition.
Stott, P., 2016. How climate change affects extreme weather events. Science 352, 1517–1518.
Talafre, J., Knabe, F., 2009. Climate change and water: an overview from the world water development report 3: water in a changing world, World Water Assessment Programme special report. https://unesdoc.unesco.org/ark:/48223/pf0000186318.locale=en.
Toonen, W.H.J., Winkels, T.G., Cohena, K.M., Prins, M.A., Middelkoopa, H., 2015. Lower Rhine historical flood magnitudes of the last 450 years reproduced from grain-size measurements of flood deposits using End Member Modelling. Catena 130, 69–81.
Trambauer, P., Werner, M., Winsemius, H.C., Maskey, S., Dutra, E., Uhlenbrook, S., 2015. Hydrological drought forecasting and skill assessment for the Limpopo River basin, southern Africa. Hydrol. Earth Syst. Sci. 19, 1695–1711.
Trigg, M.A., Birch, C.E., Neal, J.C., Bates, P.D., Smith, A., Sampson, C.C., Yamazaki, D., Hirabayashi, Y., Pappenberger, F., Dutra, E., et al., 2016. The credibility challenge for global fluvial flood risk analysis. Environ. Res. Lett. 11, 094014.
Vanniere, B., Magny, M., Joannin, S., Simonneau, A., Wirth, S.B., Hamann, Y., Chapron, E., Gilli, A., Desmet, M., Anselmetti, F.S., 2013. Orbital changes, variation in solar activity and increased anthropogenic activities: controls on the Holocene flood frequency in the Lake Ledro area, Northern Italy. Clim. Past 9 (1193–1109).
Vicente-Serrano, S.M., Beguería, S., López-Moreno, J.I., 2010. A multiscalar drought index sensitive to global warming: the standardized precipitation evapotranspiration index. J. Clim. 23 (7), 1696–1718.
Vorster, C.J., 2005. Simplified Geology, Selected Mines and Mineral Deposits-South Africa, Lesotho and Swaziland. Council of Geoscience, South Africa.
Walling, D.E., Fang, D., 2003. Recent trends in the suspended sediment loads of the world's rivers. Glob. Planet. Chang. 39, 111–126.
Weltje, G.J., Prins, M.A., 2007. Genetically meaningful decomposition of grain-size distributions. Sediment. Geol. 202, 409–424.
Wessels, K.J., Prince, S.D., Frost, P.E., van Zyl, D., 2004. Assessing the effects of human-induced land degradation in the former homelands of northern South Africa with a 1 km AVHRR NDVI time-series. Remote Sens. Environ. 91, 47–67.
Willems, P., 2009. A time series tool to support the multi-criteria performance evaluation of rainfall-runoff models. Environ. Model Softw. 24, 311–321.
Wirth, S., Gilli, A., Simonneau, A., Ariztegui, D., Vannière, B., Glur, L., Chapron, E., Magny, M., Anselmetti, F.S., 2013. A 2000-year long seasonal record of floods in the Southern European Alps. Geophys. Res. Lett. 40, 1–5.
Wu, W., Li, Y., Luo, X., Zhang, Y., Ji, X., Li, X., 2019. Performance evaluation of the CHIRPS precipitation dataset and its utility in drought monitoring over Yunnan Province, China. Geomat. Nat. Haz. Risk 10, 2145–2162.